Implications of Compensating Property-Owners for Geologic Sequestration of CO_2

R. Lee Gresham,*[,†] Sean T. McCoy,[†] Jay Apt,[†,§] and M. Granger Morgan[†]

Carnegie Mellon University, [†]Department of Engineering & Public Policy and [§]Tepper School of Business
5000 Forbes Avenue, Baker Hall 129
Pittsburgh, PA 15213

*Corresponding author phone: (412) 953-4617; fax: (412) 268-3757;
email: rgresham@andrew.cmu.edu

Supporting Information

Model Input Parameters

The model requires eight input parameters: formation depth, net thickness, porosity, permeability, salinity, temperature and pressure. Formation thickness, porosity, permeability, and depth can vary by several orders of magnitude among and within reservoirs and have large effects on injections rates. The parameterized and deterministic inputs to the model are show in Table S1.

Formation Depth, Net Thickness, Porosity and Salinity. Formation depth is the depth of the geological formation below the surface (meters). Formation thickness is the net thickness of the permeable zones of the geological formation (meters). Net thickness is used because formations typically have zones of high permeability inter-layered with low-permeability zones. Effective porosity is the percentage of the volume of connected pores in a unit volume of the formation. Porosity generally decreases with depth *(1)*, but in this case, no statistically significant

correlation between porosity and depth exists in the data for the four Pennsylvania and Ohio sandstones analyzed in this paper. Since the net thickness of high-permeability zones is used in this model, the effective porosity of high permeability zones is also used here. Salinity is the amount of dissolved NaCl in the interstitial pore water in the target formation, expressed as part per million by weight (ppm).

Formation Pressure. The relationship between pressure and depth is modeled as linear under hydrostatic conditions. At hydrostatic conditions, pressure typically increases at approximately 10 MPa/km. The relationship is expressed as:

$$P_d = G_p d + P_a \quad [MPa]$$

where P_d is pressure as a function of depth, G_p is the hydrostatic pressure gradient, 10 MPa/km, d is formation depth, and P_a is atmospheric pressure.

Formation Temperature. The relationship between temperature and depth is also modeled using a linear approximation. The average geothermal gradient is assumed to be approximately 25°C/km, but because actual temperature gradients vary somewhat from one region to another, a triangular distribution is assigned to the geothermal gradient for Monte Carlo simulations carried out in this analysis (see Table S1). The relationship between temperature and depth is expressed as:

$$T_d = G_T d + T_s \quad [K]$$

where T_d is temperature as a function of depth, G_T is the geothermal gradient, d is formation depth, and T_s is the surface temperature.

Table S1: Model Input Parameters

	Depth (m)	Net Thickness (m)	Porosity (%)	Salinity (ppm)	Irreducible Brine Saturation (%)	CO_2 Saturation[2] (%)	Temperature Gradient (°C/km)
Frio Sandstone (TX)							
Deterministic	1,900	300	30	100,000	30%	70%	25
Mt. Simon Sandstone (IL)							
Deterministic	2,300	90[1]	13	125,000	30%	70%	25
Medina Sandstone (PA)							
Triangular: Min	810	10	3%	100,000	30%	70%	20
Max	2,000	57	18%	250,000	90%	10%	50
Mode	1,500	20	8%	190,000	60%	40%	30
Volant Field							
Deterministic	1,800	26	18%	230,000	30%	70%	25
Oriskany Sandstone (PA)							
Triangular: Min	2,000	10	2%	250,000	30%	70%	20
Max	2,800	41	10%	350,000	90%	10%	50
Mode	2,700	13	5%	340,000	60%	40%	30
Clinton Sandstone (OH)							
Triangular: Min	830	11	7%	100,000	30%	70%	20
Max	1,700	20	10%	210,000	90%	10%	50
Mode	1,100	11	8%	130,000	60%	40%	30
E. Canton Consol.-S Field							
Deterministic	1,600	13	8%	200,000	30%	70%	25
Rose Run Sandstone (OH)							
Triangular: Min	830	10	8%	100,000	30%	70%	20
Max	2,300	12	10%	280,000	90%	10%	50
Mode	1,600	11	8%	200,000	60%	40%	30
Baltic Field							
Deterministic	1,900	12	10%	240,000	30%	70%	25

[1]To provide a conservative estimate that accounts for uncertainty with respect to permeability and porosity in the Mt. Simon Sandstone at the Mattoon site, half the value of the gross thickness reported by the Illinois Geological Survey was used in our analysis *(2,3,)*.
[2]CO_2 saturation is not actually an input parameter to the plume distribution model, but rather the outcome resulting from the assumed parameterized irreducible brine saturation.

Irreducible Brine Saturation

Brennan and Burruss note that as the interstitial pore water that is not displaced by injected CO_2 (i.e., irreducible brine) in the sequestration reservoir increases, storage capacity (in mass per unit volume) decreases, and the areal extent of the CO_2 plume becomes larger *(4)*. Brennan and Burruss performed their storage capacity analysis applying irreducible water saturations at 5%, 50%, 75%, and 100% *(4)*. Numerical simulations of CO_2 plume migration in the Frio injection project best match the observed behavior at irreducible brine saturations of between 15% and

30% *(5)*. Therefore, values for irreducible brine saturation were parameterized [Triangular (90,30,60)] and input into the model.

CO_2 Plume Distribution Model: Analytical Solution Derivation *(6)*

Model predictions depend largely on the values of key parameters, which describe the properties of the formation and native fluids. Multiphase models solve a series of governing equations to predict the composition and volumetric fraction (i.e., the fraction of the formation pore space taken up by fluid) of each phase state (e.g., liquid, gas, supercritical fluid), as well as fluid pressures, as a function of location and time for a particular set of conditions.

The results obtained by Nordbotten et al. *(2)* agree broadly with Buckley-Leverett theory for small values of the dimensionless gravity factor, Γ. For convenience, their result is derived here using the similar assumptions—namely, effects of capillary pressure are negligible, fluids are incompressible, and the reservoir petrophysical properties are homogeneous—using arguments analogous to those used by Dake *(7)* for an unstable, horizontal displacement.

For a differential cylindrical volume of the system shown in Figure 1 of the paper, the volumetric balance on the CO_2 phase can be written:

$$\varphi \frac{\partial \overline{S}_c(r,t)}{\partial t} + \nabla \cdot q_c(r,t) = 0 \qquad \text{(Eq. S1)}$$

where: $\overline{S}_c$ is the vertically averaged saturation of CO_2, φ is the reservoir porosity, q_c is the flux of CO_2, r represents radial distance from the injection well, and t is time. Assuming drainage (i.e., CO_2 is displacing brine in a brine-wet reservoir), the vertically averaged saturation of CO_2, $\overline{S}_c$, is defined as:

$$\overline{S}_c = \beta(1 - S_{wc}) \qquad \text{(Eq. S2)}$$

Darcy's law for the brine and CO_2 phases can be written as:

$$q_c = -K\beta\lambda_c \nabla p_c \qquad \text{(Eq. S3)}$$

$$q_w = -K(1-\beta)\lambda_w \nabla p_c \qquad \text{(Eq. S4)}$$

In Equations S3 and S4, K is the intrinsic permeability of the reservoir, β is the fraction of the reservoir thickness invaded by the CO_2 plume, λ_n is the mobility (k_r/u) for the CO_2 phase (c) or the brine phase (w), and ∇p is the pressure gradient.

Since the fluids are incompressible $(\nabla \cdot q = 0)$, the flux into the system equals the flux out of the system and the total apparent flux, q_t, is:

$$q_t = \frac{Q_{well}}{A} = q_c + q_w$$

where Q_{well} is the injection rate of CO_2 into the system and A is the area across which the flux occurs. Assuming capillary pressure is negligible and, therefore $\nabla p_c = \nabla p_w = \nabla p$, substituting Equations S3 and S4, we arrive at:

$$\frac{Q_{well}}{A} = -K\left[\beta\lambda_c + (1-\beta)\lambda_w\right]\nabla p \qquad \text{(Eq. S5)}$$

Solving Equation S5 for pressure gradient results in:

$$\nabla p = -\frac{Q_{well}}{KA\left[\beta\lambda_c + (1-\beta)\lambda_w\right]}$$

which can then be substituted into Equation S3 to arrive at the flux of the CO_2 phase as a function of the injection rate.

$$\nabla p = \frac{\beta\lambda_c}{\beta\lambda_c + (1-\beta)\lambda_w}\left(\frac{Q_{well}}{A}\right) = f_c\frac{Q_{well}}{A} \qquad \text{(Eq. S6)}$$

In Equation S6, the term referred to as f_c is the fractional flow of the carbon dioxide phase in the system. Substituting this equation into the volumetric balance, Equation S1 yields:

$$\varphi\frac{\partial\overline{S}_c}{\partial t} + \nabla\cdot\left(f_c\frac{Q_{well}}{A}\right) = 0$$

Writing the divergence operator for a cylindrical coordinate system gives:

$$\varphi\frac{\partial\bar{S}_c}{\partial t}+\frac{1}{r}\frac{\partial}{dr}\left(rf_c\frac{Q_{well}}{2\pi rh}\right)=0$$

Simplifying results in:

$$\varphi\frac{\partial\bar{S}_c}{\partial t}+\frac{Q_{well}}{2\pi rh}\frac{\partial f_c}{dr}=0 \qquad \text{(Eq. S7)}$$

Applying the chain rule to the fractional flow equation, the $\partial f_c/dr$ can be rewritten:

$$\frac{\partial f_c}{dr}=\frac{\partial f_c}{d\bar{S}_c}\times\frac{\partial\bar{S}_c}{\partial r}=f_c'\frac{\partial\bar{S}_c}{\partial r}$$

Upon substitution into Equation S7, we arrive at a statement of the Buckley-Leverett equation for a radial system:

$$\frac{\partial\bar{S}_c}{\partial t}+\frac{Q_{well}f_c'}{2\pi rh\varphi}\frac{\partial\bar{S}_c}{\partial r}=0 \qquad \text{(Eq. S8)}$$

This equation was solved by Woods and Comer *(8)* for the boundary conditions $r = r_w$ at $t = 0$, resulting in:

$$r\left(\bar{S}_c\right)=\sqrt{\frac{f_c'Q_{well}t}{\pi h\varphi}+r_w^2} \qquad \text{(Eq. S9)}$$

If vertically averaged saturation of the CO_2 phase was not assumed (i.e., Eq. S4), determination of f_c' would require an assumption of the shape of the relative permeability curves for the CO_2-brine system and particular reservoir rock. However, operating under the assumption saturation is a linear average of phase saturations (i.e., Eq. S2), f_c' can be expressed via the chain rule as:

$$f_c'=\frac{df_c}{\partial\beta}\times\frac{\partial\beta}{d\bar{S}_c}=\frac{\lambda_w\lambda_c}{\left[\lambda_w+\beta\left(\lambda_c-\lambda_w\right)\right]^2}\left(\frac{1}{1-S_{wc}}\right)$$

Substituting this into the above equation, we arrive at an expression for the radial distance as a function of the fraction of the formation height invaded by the CO_2 plume:

$$r(\beta) = \sqrt{\frac{\lambda_w \lambda_c Q_{well} t}{\pi h \varphi (1 - S_{wc}) \left[\lambda_w + \beta(\lambda_c - \lambda_w)\right]^2} + r_w^2} \qquad \text{(Eq. S10)}$$

Assuming the injection well radius is much smaller than the radius of the CO_2 plume, the maximum extent of the CO_2 plume occurs at $\beta = 0$:

$$r_{\max} = \sqrt{\frac{\lambda_c V}{\pi h \varphi \lambda_w (1 - S_{wc})}} \quad [m] \qquad \text{(Eq. S11)}$$

In the situation where the dimensionless gravity factor, Γ, is large, the solution presented in Equation S11 under predicts the extent of migration of the CO_2-brine interface. However, after incorporating the effects of buoyancy into the derivation (and making the same assumptions as above) Nordbotten et al. arrived at:

$$r_{\max} = \sqrt{\frac{(\lambda - 1)V}{2\pi \Lambda h \varphi (1 - S_{wc})}} \quad [m] \qquad \text{(Eq. S12)}$$

where λ is the mobility ratio for the displacement (λ_c / λ_w), and Λ is the Lagrangian multiplier. The Lagrangian multiplier, Λ, comes from the numerical solution of:

$$\Lambda(\lambda - 1)^2 - \Gamma(\lambda - 1) + \Gamma\lambda \ln\left(\frac{\Gamma + \Lambda}{\Lambda\lambda}\right) = \frac{2\lambda\left[\Lambda(\lambda - 1) - \Gamma\right]^2}{\lambda - 1} \qquad \text{(Eq. S13)}$$

Estimated Oil & Gas Field CO_2 Sequestration Capacities in the MRCSP Region

Table S2: Oil & Gas Field CO_2 Sequestration Capacities in the MRCSP Region *(9,10)*

Producing Formation	Field Name	State	Field Size (km^2)	GS Potential (million tonnes)
Medina	Volant	PA	130	310
Clinton	E. Canton Consolidated-S	OH	490	250
Rose Run	Baltic	OH	340	230

CO_2 Plume Size Results

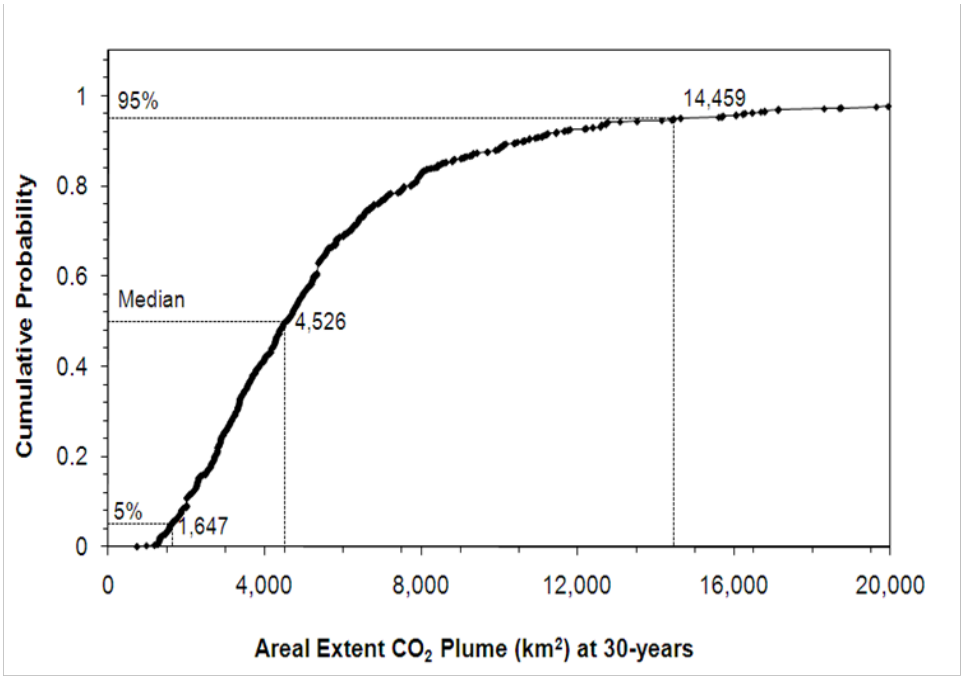

Figure S1: Medina Sandstone estimated CO_2 plume footprint using the Nordbotten et al. solution.

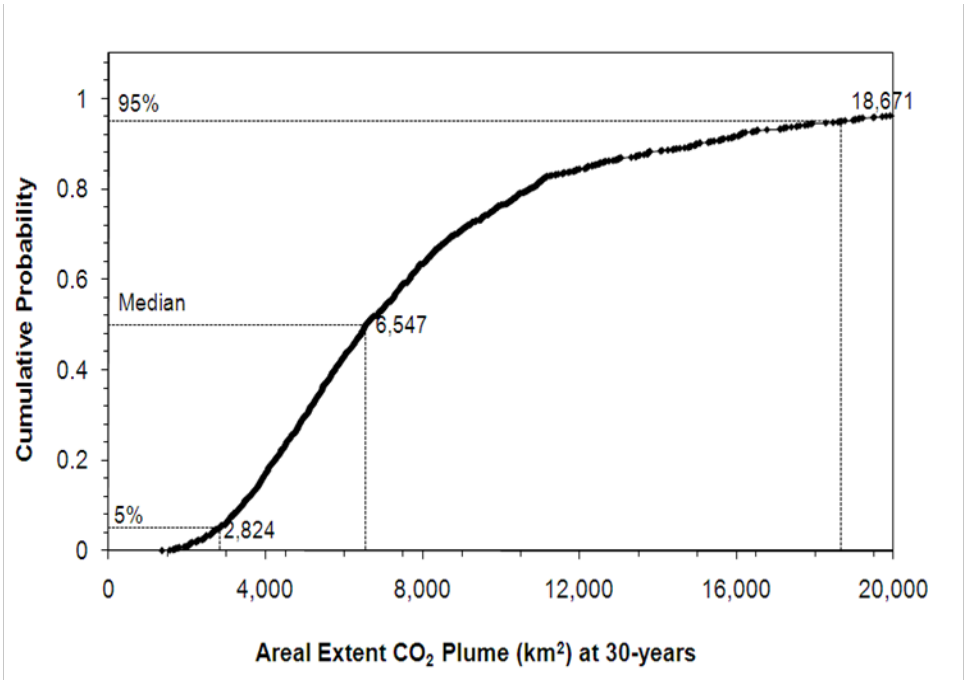

Figure S2: Oriskany Sandstone estimated CO_2 plume footprint using the Nordbotten et al. solution.

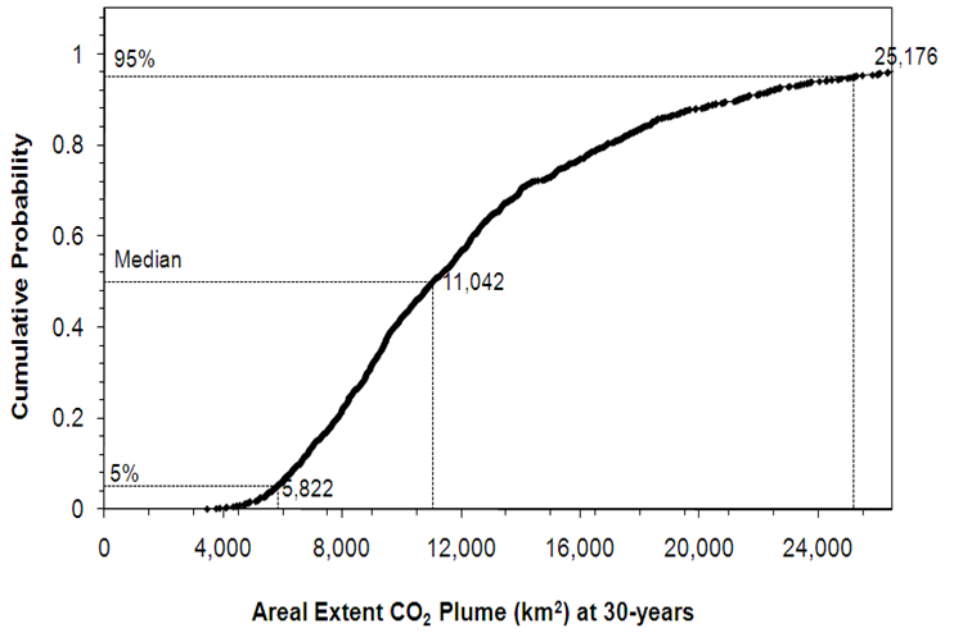

Figure S3: Clinton Sandstone estimated CO_2 plume footprint using the Nordbotten et al. solution.

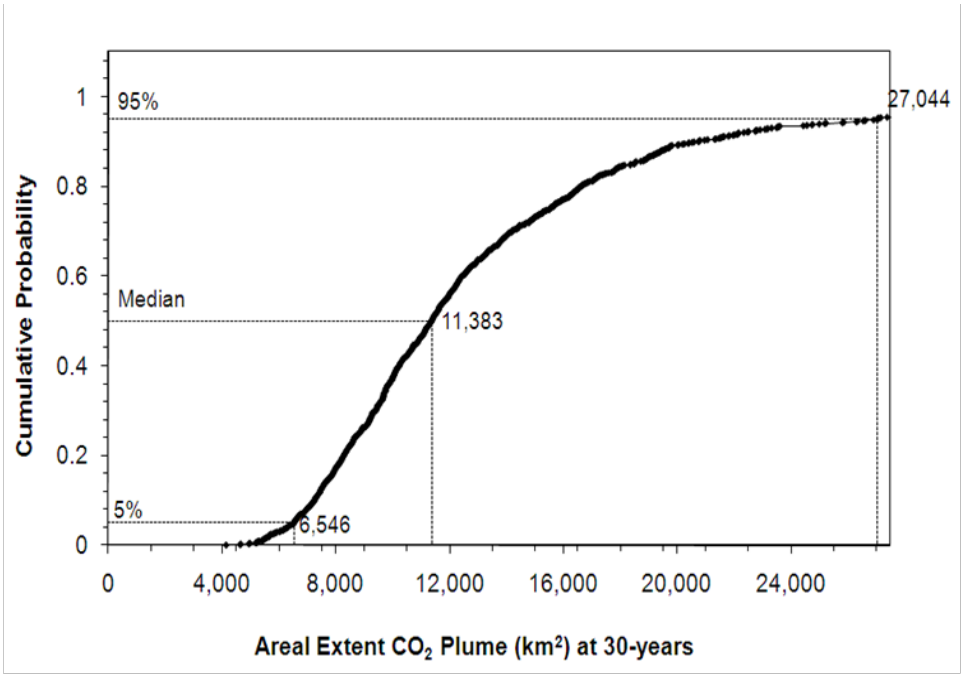

Figure S4: Rose Run Sandstone estimated CO_2 plume footprint using the Nordbotten et al. solution.

CO_2 Plume Model Sensitivity

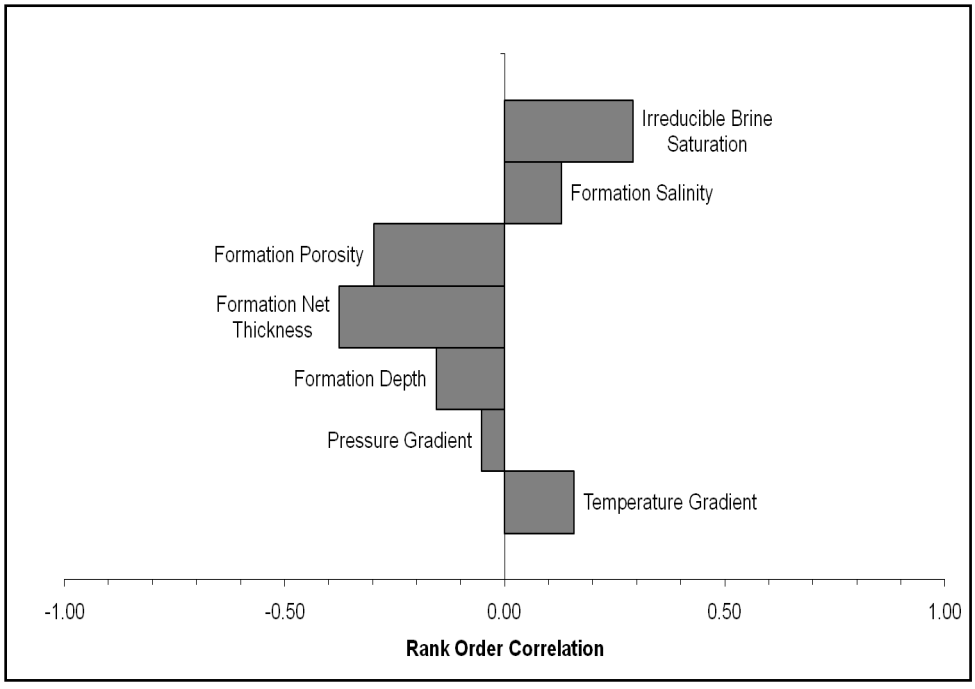

Figure S5: Medina Sandstone rank order correlation between the results of the Monte Carlo sensitivity analysis and the parameters assigned triangular distributions.

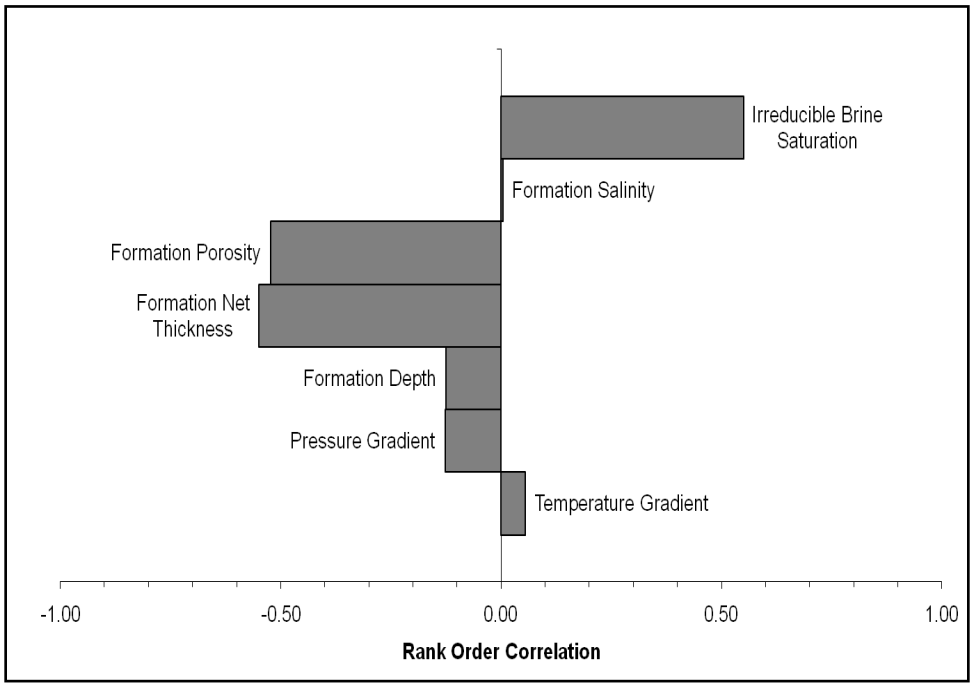

Figure S6: Oriskany Sandstone rank order correlation between the results of the Monte Carlo sensitivity analysis and the parameters assigned triangular distributions.

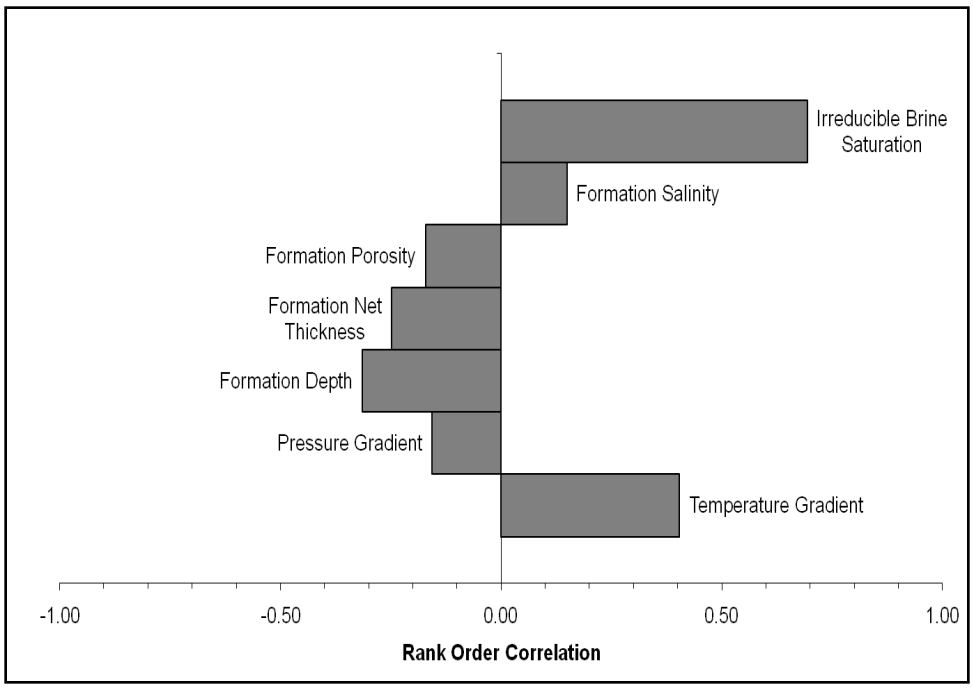

Figure S7: Clinton Sandstone rank order correlation between the results of the Monte Carlo sensitivity analysis and the parameters assigned triangular distributions.

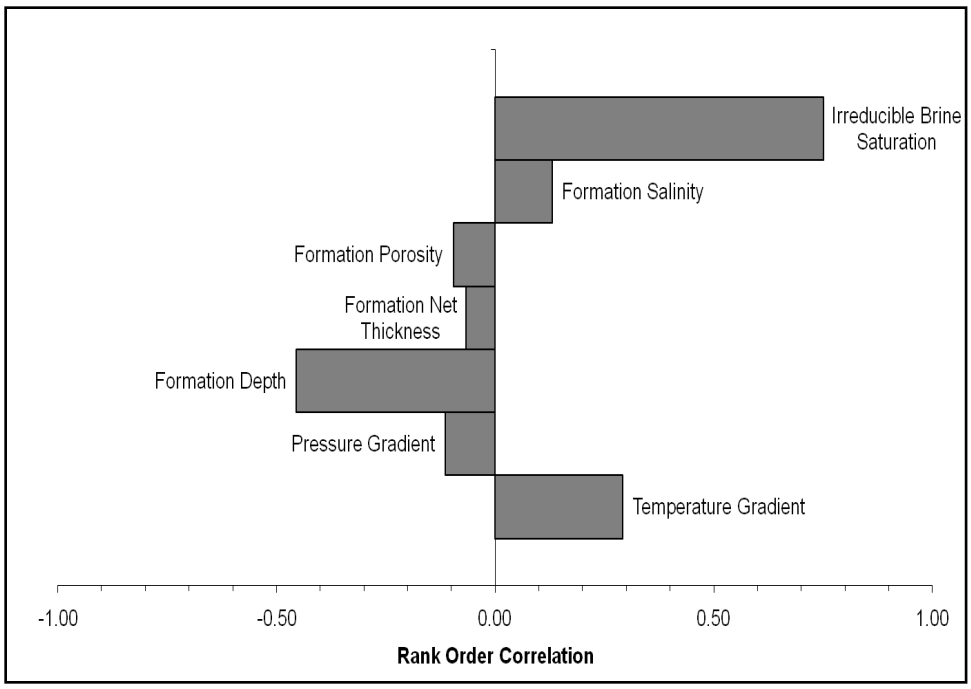

Figure S8: Rose Run Sandstone rank order correlation between the results of the Monte Carlo sensitivity analysis and the parameters assigned triangular distributions.

Distribution of Pore Space Acquisition Costs

The value of the one-time payment for the long-term lease is assumed to be $500, the equivalent sum paid to landowners in Illinois for the option to lease pore space rights for the FutureGen™ Alliance project *(11)*. Even if as many as 120 (the number assumed for this paper) landowners fall within the areal extent of the CO_2 plume, the $60,000 expenditure to secure the option to lease is insignificant compared to the total lease cost. If the CO_2 plume underlies more densely populated areas, the option cost would no longer be insignificant. Because GS developers will only acquire a servitude (i.e., the "right to use") under a lease instrument instead of a fee title (i.e., the full possessory right) if sequestration rights are purchased, it makes sense that, on balance, less compensation will be paid for a sequestration lease than a full fee interest in the pore space

Table S3: Present Value 100-year Lease Cost vs. Purchase Cost (millions 2009$)[1]

	Annual Lease[a]		Long-Term Lease[b]		Purchase Cost[b]	
	Private	*State*	*Private*	*State*	*Private*	*State*
Medina (PA)						
5th Percentile	$7.6-41	$180-270	$2.5-13	$50-79	$8.3-45	$170-270
Median	$21-110	$500-700	$6.8-35	$140-200	$23-120	$490-690
95th Percentile	$62-350	$1,500-2,200	$20-110	$440-640	$67-380	$1,500-2,200
Oriskany (PA)						
5th Percentile	$13-61	$280-400	$4.2-20	$80-120	$14-66	$270-400
Median	$33-150	$700-1,000	$11-49	$200-300	$36-170	$680-1,000
95th Percentile	$91-420	$1,900-2,800	$29-130	$540-830	$98-460	$1,800-2,800
Clinton (OH)						
5th Percentile	$27-130	$610-860	$8.7-42	$170-250	$29-140	$590-860
Median	$49-260	$1,100-1,600	$16-82	$320-490	$54-280	$1,100-1,700
95th Percentile	$120-620	$2,900-3,700	$38-200	$820-1,200	$130-670	$2,800-3,700
Rose Run (OH)						
5th Percentile	$28-140	$640-930	$9.1-46	$180-270	$31-160	$620-940
Median	$52-260	$1,200-1,700	$17-84	$330-500	$57-290	$1,100-1,700
95th Percentile	$120-590	$2,700-3,900	$40-190	$760-1,100	$140-640	$2,600-3,900

[1]Assumes 15% discount rate and 4% inflation rate.
[a]Annual lease rate range $2-10 per acre per year for private land, and $45-65 per acre per year for private land.
[b]Long-term lease rate and purchase cost range $20-100 per acre for private land, and $400-600 per acre for state-owned land.

Pipeline Model Design and Assumptions

Operating pressures throughout the pipeline remain above 10.3 MPa to ensure the CO_2 does not fall into a subcritical state *(12,13)*. Injection pressure, booster compressors, and pipeline diameter all influence pipeline pressure. A fixed size is assumed for both injection and booster compressors. To ensure CO_2 remains supercritical throughout the pipeline, the required diameter for a pipeline segment is sized according to operating parameters such as pressure drop, CO_2 density and mass flow rate, and frictional losses *(12,14)*. Pipeline diameter is calculated while holding the upstream and downstream pressures constant *(12)*. Depending on the pipeline length,

additional pumping stations might be required to boost the pressure along the pipeline to compensate for pressure losses *(12,14)*. It is assumed a booster station is required when the length of a pipeline segment exceeds 205 miles (402 km).

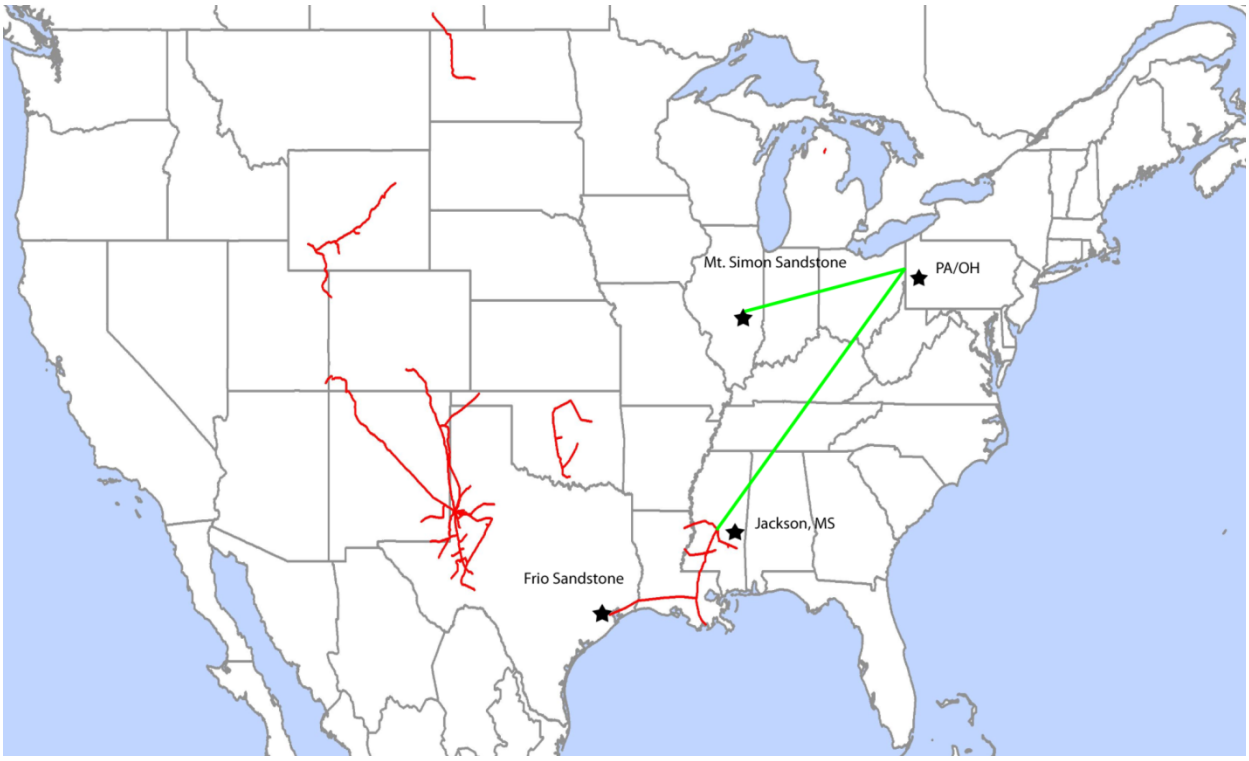

Figure S9: Pipeline from PA/OH to the Mt. Simon and Frio Sandstones *(15)*. Red lines represent existing CO_2 pipeline infrastructure; the green lines represent the hypothetical pipeline scenarios we assess in this paper.

Pipeline Model Annualized Costs

Table S4: Pipeline Annualized Costs

	Pipeline Length		Proportion of Total Pipeline Length	Annualized Cost	
	(km)	(miles)	(%)	($/yr)	($/tonne)
Volant, PA to Mattoon, IL (2 segments; 1 booster station)					
Northeast Region	20	12	3%	$47,000,000	$8.6
Capital Cost				$44,000,000	
Operational Cost				$2,500,000	
Energy Cost for Booster				$500,000	
Midwest Region	690	429	97%	$41,000,000	$7.5
Capital Cost				$38,000,000	
Operational Cost				$2,500,000	
Energy Cost for Booster				$500,000	
Total	710	441		$41,180,000	$7.6
Volant, PA to Jackson, MS (4 segments; 3 booster stations)					
Northeast Region	20	12	1%	$117,000,000	$21.5
Capital Cost				$109,000,000	
Operational Cost				$6,450,000	
Energy Cost for Booster				$1,000,000	
Midwest Region	310	193	16%	$103,000,000	$18.9
Capital Cost				$96,000,000	
Operational Cost				$6,450,000	
Energy Cost for Booster				$1,000,000	
Southeast Region	970	603	49%	$113,000,000	$20.8
Capital Cost				$105,000,000	
Operational Cost				$6,450,000	
Energy Cost for Booster				$1,000,000	
Jackson, MS to TX Gulf Coast (No new construction required)					
Southeast Region	160	99	8%	$7,400,000	$1.4
Operational Cost				$6,450,000	
Energy Cost for Booster				$1,00,000	
Southwest Region	540	336	27%	$7,400,000	$1.4
Operational Cost				$6,450,000	
Energy Cost for Booster				$1,000,000	
Total	1,860	808		$74,526,000	$13.7

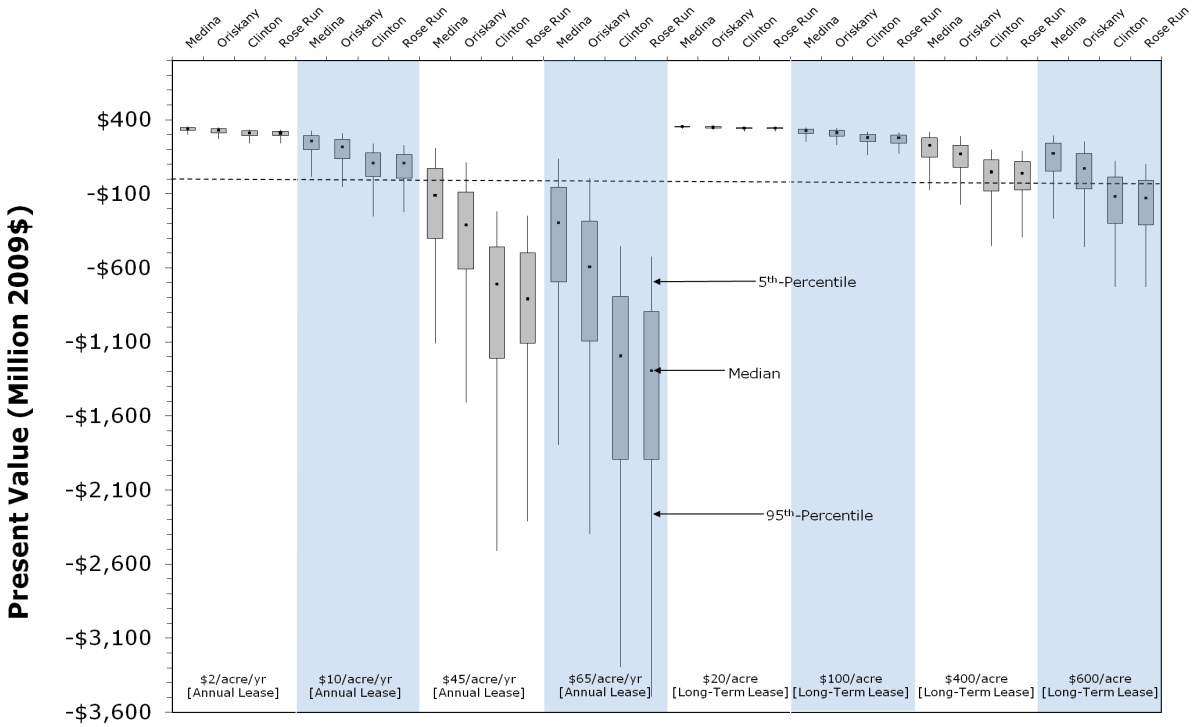

Figure S10: Difference between the sum of the Mattoon 30-year pipeline operation cost & 100-year pore space lease cost and the MRCSP sandstone pore space lease costs.

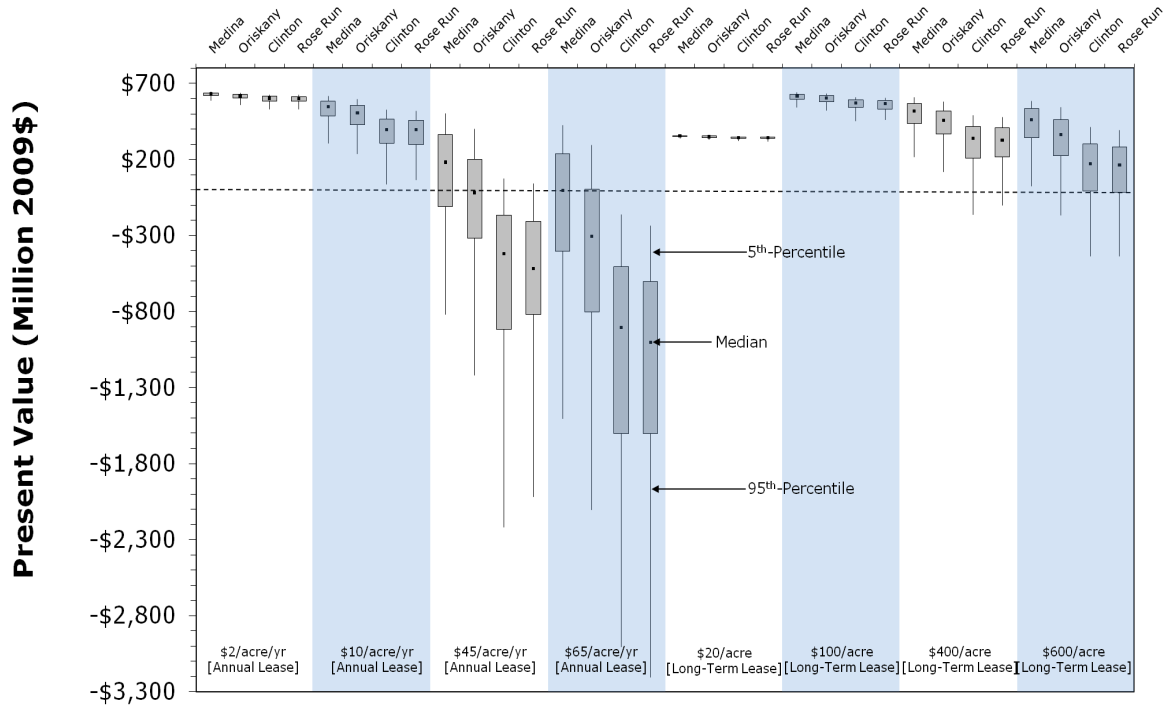

Figure S11: Difference between the sum of the Frio 30-year pipeline operation cost & 100-year pore space lease cost and the MRCSP sandstone pore space lease costs.

Literature Cited

(1) Athy, L.F. Density, porosity, and compaction in sedimentary rocks. *AAPG Bulletin*. **2005**, *14*(1), 1-24.

(2) FutureGen Industrial Alliance: Mattoon site environmental information volume 2007. Available at http://www.futuregenalliance.org/news/evi.stm (accessed November 14, 2008).

(3) Wise, P.; Coal Information Coordinator Office of Coal Development, Illinois Department of Commerce and Economic Opportunity, Personal Communication (*Mattoon, IL subsurface geology proposal obtained via email correspondence.*), 2008.

(4) Brennan, S.T.; Burruss, R.C. Specific storage volumes: A useful tool for CO_2 storage capacity assessment. *Natural Resources Research*. **2006**, *15*(3), 165-182.

(5) Doughty, C.; Freifeld, B. M.; Trautz, R. C. Site characterization for CO_2 geologic storage and vice versa: the Frio brine pilot, Texas, USA as a case study. *Environ.Geol.* **2008**, *54*(8), 1635-1656.

(6) McCoy, S.T. *The Economics of CO_2 transport by pipeline and storage in saline aquifers and oil reservoirs*; Carnegie Mellon University: Pittsburgh, PA, 2008. Available at http://wpweb2.tepper.cmu.edu/ceic/publications.htm (accessed August 10, 2009).

(7) Dake, L.P. *Fundamentals of Reservoir Engineering*; Elsevier Science: New York, 1983.

(8) Woods, E.G.; Comer, A.G. Saturation distribution and injection pressure for a radial gas-storage reservoir. *Journal of Petroleum Technology*. **1962**, *14*(12), 1389-1393.

(9) U.S. Department of Energy National Energy Technology Laboratory. *Carbon Sequestration Atlas of the United States and Canada*; DOE: Washington, DC, 2007.

Available at http://www.netl.doe.gov/technologies/carbon_seq/refshelf/atlas/ (accessed December 10, 2008).

(10) Midwest Regional Carbon Sequestration Partnership: *Characterization of Geologic Sequestration Opportunities in the MRCSP Region* in Phase I Final Report; MRCSP: Columbus, OH, 2005.

(11) Moody, B.; Executive Director Tuscola Economic Development, Inc. Personal Communication, 2008.

(12) McCoy, S.T.; Rubin, S.T. An engineering economic model of pipeline transport of CO_2 with application to carbon capture and storage. *Int. J. Greenhouse Gas Control*. **2008**, *2*(2)**,** 219-229.

(13) Bock, B.; Rhuddy, R.; Herzog, H.; Klett, M.; Davison, J.; De La Torre Ugart, D.G.; Simbek, D. Economic evaluation of CO_2 storage and sink enhancement options. *Final Technical Report to the U.S. Department of Energy*. TVA Public Power Institute: Muscle, Shoals, AL, 2003.

(14) Newcomer, A.; Apt, J. Implications of generator siting for CO_2 pipeline infrastructure. *Energy Policy*. 2008, *36*,1776-1787.

(15) *Global Energy Decision Velocity* Suite; Ventyx: Atlanta, GA, 2009. Available at http://www.ventyx.com.